Ion Exchange Conversion of Na-birnessite to Mg-buserite for Enhanced Cu^{2+} Removal via Membrane Capacitive Deionization (MCDI)

Feihu Li*, Yang Bao, Jie Jin, and Man Li

Collaborative Innovation Center of Atmospheric Environment and Equipment Technology, Jiangsu Key Laboratory of Atmospheric Environment Monitoring and Pollution Control, School of Environmental Science and Engineering, Nanjing University of Information Science and Technology, Nanjing 210044, China

* Corresponding author.

E-mail address: fhli@nuist.edu.cn (F. Li).

1

Abstract

Layered manganese oxides (LMOs) have recently been demonstrated to be one of the most promising redox-active material platforms for electrochemical removal of heavy metal ions from solution via capacitive deionization (CDI). However, the impacts of phase transformation behaviors of the LMOs minerals, especially during the desalination operations, on the deionization performance of the LMOs/C electrodes have yet to be extensively evaluated. In this study, Mg-buserite derived from ion exchange of fresh Na-birnessite, Na- and K-birnessite were systematically evaluated as active electrode materials for removal of copper (Cu^{2+}) ions from synthetic saline in a symmetric membrane capacitive deionization (MCDI) cell. In the cases of Na^+, K^+, Mg^{2+}, and Ca^{2+} ions, the Mg-buserite/C electrode demonstrated the best deionization performance in terms of the salt and/or ion adsorption capacity, electrosorption rate, charge efficiency, and cycling stability, followed by K-birnessite/C, and then Na- birnessite/C. More importantly, the Mg-buserite/C electrode also exhibited the highest Cu^{2+} ion adsorption capacity (IAC) of 89.3 mg Cu^{2+}/g active materials at a cell potential of 1.2 V in 500 mg L^{-1} $CuCl_2$ solution, with an IAC retention as high as 96.3% after 60 electrosorption/desorption cycles. The underlying mechanisms for Cu^{2+} sequestration were investigated via *ex-situ* X-ray diffraction, indicating that the improving deionization performance toward Cu^{2+} from solution is mainly attributed to the expanded interlayer spacing through ion exchange of the original stabilizing Na^+ ions of Na-birnessite with foreign Mg^{2+} ions, leading to a phase transformation from Na-birnessite into Mg-buserite that has larger ion diffusion channels and a higher ion storage capacity. Our work has demonstrated that expansion of interlayer spacing of LMOs minerals via ion exchange is a reliable and solid strategy for improving the desalination performance in CDI platforms, and provided insight for the rational design of smart electrodes for CDI applications towards heavy metal ion sequestration.

INTRODUCTION

Water scarcity and anthropogenic pollution worldwide has aroused a wide variety of global issues relevant to public health, agriculture, industrial production, ecosystems, as well as the sustainability of our society.[1,2] Heavy metal ions have been commonly found in both groundwater and surface waters, and categorized as toxic contaminants of public health and environmental concern. Copper ion (Cu^{2+}), in particular, is identified as one of the fourteen toxic heavy metals due to its adverse effect on human health especially when ingested in excess. Major anthropogenic sources of Cu^{2+} in surface waters include mining, hydrometallurgy, metal plating, printing circuit, fertilizer, and refining industries.[3-6] The permissible limits in the World Health Organization (WHO)'s standard for Cu^{2+} discharged into surface water and in drinking water are 3.0 and 0.05 mg L^{-1}, respectively. Conventional approaches for Cu^{2+} removal from aqueous solution include ion exchange, adsorption, membrane filtration, and chemical precipitation.[4,7] These processes are often limited and costly due to the need for regeneration with excessive chemicals and/or massive clean water for backwashing, and extra cost in dealing with the chemical sludge. It is therefore of great importance for boosting the innovation of robust new methods of sequestering Cu^{2+} at lower cost and without the use of chemicals and the impact on the environment.

Recently, capacitive deionization (CDI) has been demonstrated as a promising technique for ion separations, offering an attractive and prospective platform for desalination,[8-10] selective ion removal,[11-14] and recovery of high-value elements.[13-16] Carbon-based materials such as carbon aerogels, activated carbon, carbon nanotubes, carbon nanofibers, graphene, mesoporous carbon, and carbide-derived carbon are the most widely used electrodes for the removal of ions (e.g., Na^+, Cl^-, and heavy metals) from aqueous solutions via ion electrosorption and the formation of Helmholtz electric double layer (EDL) inside the CDI cells.[3,6,17-21] More recently, it has been shown that hybridization of the conventional carbon electrodes with Faradaic/redox-active materials can greatly enhance the salt adsorption capacity (SAC) and selectivity for heavy metal ions (e.g., Cu^{2+}, Pb^{2+}, etc.),[4,5,22-26] as a greater amount of heavy metal ions are stored pseudocapacitively or intercalatively in addition to ions electrosorbed by the pristine carbon electrodes. For instance, Liu et al.[22] reported that electrodeposition of a manganese dioxide (MnO_2) film onto carbon fiber (CF) can significantly improve its SAC for Cu^{2+}. The resultant MnO_2/CF electrode exhibited a maximum

Cu^{2+} adsorption capacity as high as 172.88 mg g^{-1}. Zhang et al. [25] developed a redox-active molybdenum dioxide/carbon spheres (MoO$_2$/C) electrode for selective removal of Pb^{2+} by an asymmetric CDI method. The MoO$_2$/C electrode displayed a high Pb^{2+} removal efficiency of >99% in a mixture of 100 ppm Pb(NO$_3$)$_2$ and 100 ppm NaCl and high regeneration performance in such mixed solutions. Besides, zinc sulfide (ZnS),[5] titanium dioxide (TiO$_2$),[27] ferriferous oxide (Fe$_3$O$_4$),[24] have all been employed as dopants for carbon electrodes used in CDI apparatus.

Layered manganese oxides (LMOs), i.e., the birnessite-buserite family of layered MnO$_2$ have gained fast-growing interest as active electrode materials for both electrochemical supercapacitors and CDI, principally due to their high theoretical specific capacitance (i.e., 1370 F g^{-1}), abundance, low-cost, and environmental benignity.[4, 23, 28-36] Birnessite, in particular, has been extensively studied as CDI electrode materials for enhanced electrosorption of sodium (Na$^+$) [31-34] and heavy metal ions (e.g., Cu^{2+}, Zn^{2+}, and Ni^{2+}) [4, 30, 37] due to its excellent electrochemical redox activity, large abundance of Mn(IV) vacancies in the MnO$_6$ octahedra layers, and tailorable surface and interlayer properties. On the other hand, rational expanding the interlayer spacing in layered materials has been well established as a successful strategy to improve their performance in ion sieving,[38] electrochemical energy storage,[39, 40] and Na$^+$ storage.[41] Recent works to increase the interlayer spacing of birnessite via ion exchange demonstrated enhanced ion adsorption capacities for Na$^+$.[31, 32] Ion exchange treatment of the pristine Na-birnessite (NaB) with magnesium chloride (MgCl$_2$) solution led to a phase transformation from NaB to Mg-buserite (MgB) with an interlayer spacing of ~ 9.7 Å, demonstrating a much higher SAC of 37.2 mg g^{-1} compared to that of NaB.[32] Nevertheless, the electrochemical interaction of Mg-buserite with heavy metal ions (e.g., Cu^{2+}) in a CDI platform has not yet been extensively explored.

In this study, Mg-buserite derived from ion exchange of pristine Na-birnessite, Na- and K-birnessite were utilized as active electrode materials for electrosorption of Cu^{2+} in a membrane capacitive deionization (MCDI) system, under varying salt/ion concentrations and electrochemical conditions. The Mg-Buserite/C electrode acting as both anode and cathode demonstrated much greater capacities and faster rates for removal of Cu^{2+}, and other metal ions (i.e., Na$^+$, K$^+$, Mg^{2+}, Ca^{2+}) compared to the pristine Na- and K-Birnessite/C electrodes. This benefits from its expanded interlayer spacing that can store more ions inside

the MnO_6 layers, and facilitate the ion transporting from the bulk solution into the interlayers. In addition, the Mg-Buserite/C electrode exhibited excellent cycling stability in the removal of Cu^{2+}, with little recession in SACs over 60 electrosorption/desorption cycles. Our findings are expected to serve as a platform of tailoring layered manganese oxides for enhanced capacitive deionization performance, and shed light on the correlations between the interlayer spacing, the nature of intercalating/stabilizing cations, and the deionization performance of an MCDI system toward heavy metal removal from solution.

EXPERIMENTAL SECTION

All chemicals used in this study were of reagent grade quality or above and were obtained from Sinopharm Chemical Reagent Co., Ltd. (Shanghai, China) unless otherwise specified. All solutions were prepared with deionized water (DI H_2O, resistivity $\geq$ 18 MΩ·cm at 25 °C).

Preparation and Characterization of Birnessite/Buserite Materials.

Na-birnessite (NaB) was prepared via a modified solution reaction/precipitation method (Figure 1A, Text S1 in the Supporting Information).[42] K-birnessite (KB) was prepared following the same procedure used for NaB only by replacing NaOH with KOH. Mg-buserite (MgB) was synthesized via an ion exchange approach (Figure 1A).[32] More experiment details and characterization can be found in the Supporting Information (Text S1, S2).

Electrochemical Measurements.

Cyclic voltammetry (CV), galvanostatic charge-discharge (GCD), and electrochemical impedance spectroscopy (EIS) measurements were carried out in 1.0 M NaCl solution on a CS310H electrochemical workstation (Correst, Wuhan, China) with a three-electrode system. The three-electrode configuration consists of a working electrode (1 × 1 cm^2), a platinum (Pt) foil counter electrode (1 × 1 cm^2), and an Ag/AgCl (3.0 M KCl) electrode (reference electrode). More experiment details are shown in Text S3 in the Supporting Information.

Desalination Experiments.

A symmetric MCDI device was used to determine the desalination performance of the LMOs minerals. The electrodes were prepared by coating a mixture of birnessite/buserite (~ 0.05 g), acetylene black, and PVDF with a mass ratio of 8: 1: 1 onto the graphite paper (10 × 10 cm^2) to form an active desalination area of 5 ×

119   5 cm^2 with an average thickness of ~ 0.1 mm. The detailed procedures for the CDI electrode fabrication

120   can be found elsewhere.[34] A batch-mode operation was used to run the MCDI device (Figure S1 in the

121   Supporting Information), where a total volume of 40 mL of feed saline (e.g., NaCl) with a starting

122   concentration ranging from 50 to 1000 mg L^{-1} was continuously circulated at room temperature through a

123   peristaltic pump (BT-100, Longer Precision Pump Co., China) at a flow rate of 40 mL min^{-1}. More

124   experimental details are given in the Supporting Information (Text S4).

RESULTS AND DISCUSSIONS

Physicochemical Characteristics of As-prepared LMOs.

127   Birnessite is a ubiquitous oxide mineral of manganese (III, V) in various natural environments, and the

128   naturally occurring birnessite generally contain foreign ions (i.e., Na$^+$, K$^+$, Ca^{2+}) as their intercalating

129   cations in the interlayer region.[43] To elucidate the effects of intercalating cations on the interlayer spacing

130   and thus their ion storage performance, we prepared birnessite with specific ions (i.e., Na, K) as the

131   intercalating cations via a solution reaction/precipitation method, and Mg-Buserite intercalated with

132   magnesium ions via an ion exchange approach (Figure 1A). X-ray diffraction analysis (XRD) indicated that

133   the XRD patterns of as-prepared Na-birnessite (NaB), K-birnessite (KB), and Mg-buserite (MgB) can be

134   well indexed to JCPDS Nos. 43-1456, 80-1098, and 50-0014, respectively (Figure 1B). The interlayer

135   spacings calculated from the position of (001) reflections in the XRD patterns, d_{001}, are 9.70, 7.23, and 7.18

136   Å for MgB, KB, and NaB, respectively, in good agreement with previously reported data.[32, 43] X-ray

137   photoelectron spectroscopy (XPS) surface analysis confirmed that the intercalating cations of MgB, KB,

138   and NaB are Mg^{2+}, K$^+$, and Na$^+$, respectively (Figure 1C). The two spin-orbit peaks in Mn 2p XPS spectra

139   assignable to Mn 2p$_{1/2}$, and Mn 2p$_{3/2}$ exhibited spin-orbit splitting values (ΔE) of 11.50, 11.41, and 11.50

140   eV for MgB, KB, and NaB, respectively (Figure 1D−F). Further, the Mn 3s spectra also showed spin-orbit

141   peak splitting with ΔE of 4.80, 4.86, and 4.97 eV (Figure S2B, D, F, Supporting information), indicative of

142   an oxidation state of Mn^{+4} in these samples.[23, 34, 44] The O 1s spectra (Figure S2A, C, E) can be differentiated

143   as the tetravalent oxide (Mn-O-Mn), the hydrated trivalent oxide (Mn-O-H), and the residual water

144   molecular (H-O-H).[34] This finding is in good consistency with the FTIR spectra (Figure S3), which

145   demonstrated the surface oxygen species are attributed to surface hydroxyl groups (~ 3415 cm^{-1}), water

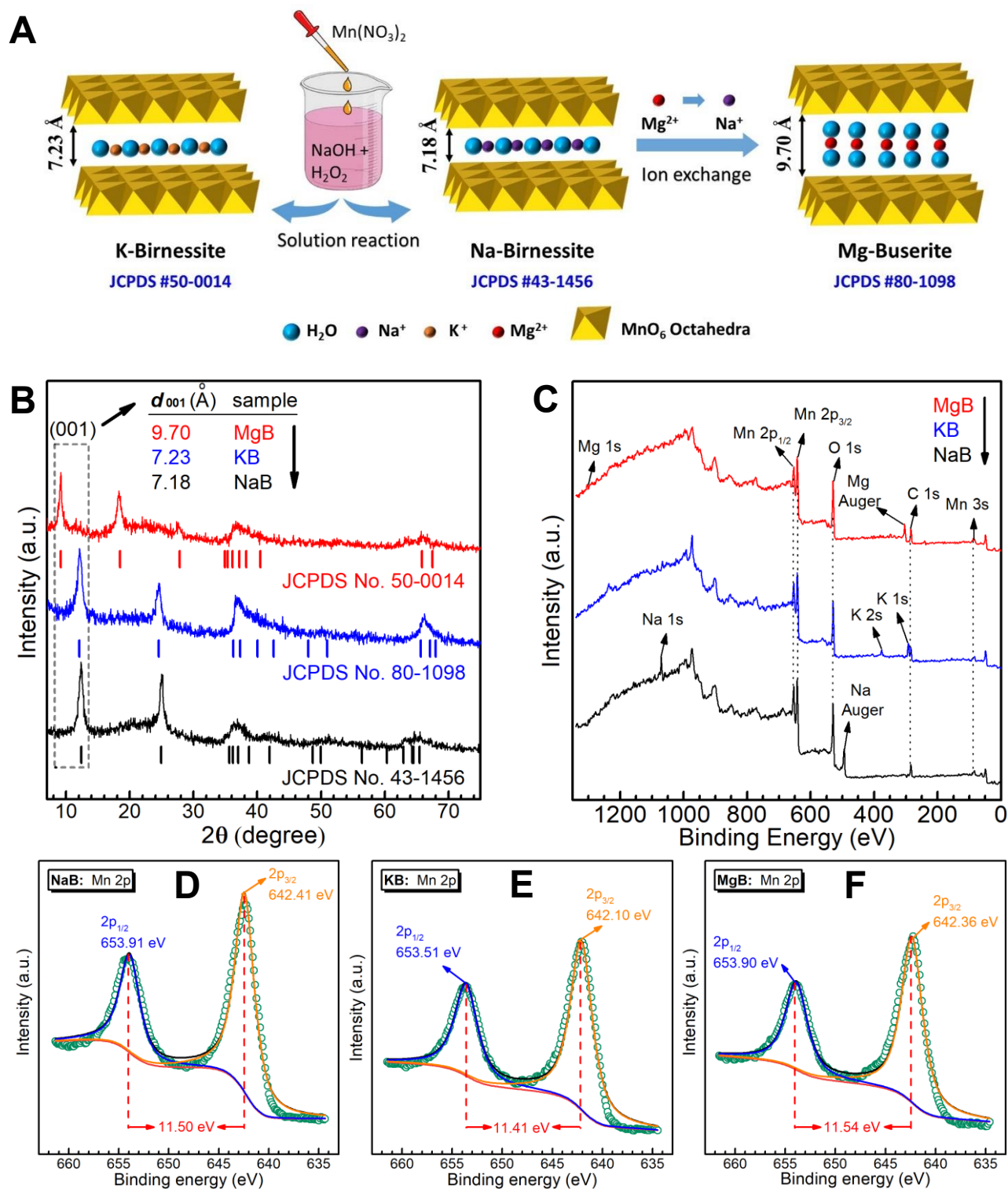vapor (~ 1617 cm^{-1}), and metal oxide (400-600 cm^{-1}).[45]

Figure 1. (**A**) Schematical illustration of the preparation of Na-, K-birnessite (NaB, KB), and Mg-buserite (MgB); (**B**) XRD patterns; (**C**) XPS survey spectra; (**D−F**) Mn 2p XPS spectra of NaB, KB, and MgB.

SEM images (Figure S4) show that these materials consisted of irregular grit stone-like particulates with mean particle sizes of 6.6, 6.1, and 6.8 μm for MgB, KB, and NaB, respectively (see the corresponding insets in Figure S4A−C), whereas the hydrothermal treated Na-Birnessite exhibited a platelet morphology stacked together (Figure S4D). Pore structure results (Figure S5) determined by the N_2 adsorption-desorption method indicate that all these samples exhibit type IV isotherms with hysteresis loops of type H2 at a high relative pressure ($P/P_0 > 0.4$) in the light of the IUPAC classification, implying that all these samples have well-defined mesopores. These results are further confirmed by the BJH pore size distribution (PSD) plots (Figure S5B), in which NaB and KB exhibited a narrow PSD centered at mean pore sizes of ∼ 23.3 and 12.6 nm, respectively, whereas MgB showed a broad PSD with two mean pore sizes of ∼26.4 and 39.2 nm. The BET specific surface areas (S_{BET}) are ∼ 75, 137, and 73 m^2 g^{-1} for MgB, KB, and NaB, respectively (Table S1, Supporting Information), which are in good assistance with the above particle size distribution data and also comparable to those in the previous reports.[4, 28, 34]

Electrochemical Performance.

The cyclic voltammetry (CV) results of these LMOs/C (i.e., birnessite/C and/or buserite/C) electrodes obtained in a 1 M NaCl solution at various scanning rates (Figure S6) exhibit leaflike-shaped voltammograms at high scanning rates (i.e., 50, and 100 mV s^{-1}), indicative of less ideal capacitive behaviors compared to carbon-based electrodes.[33, 34] Note that these CV curves are in part distorted with redox peaks over the potential window of 0−0.8 V (Figure S6D), which are derived from the Faradaic reactions of redox-active MnO_2, confirming the reversible redox activity of these composite electrodes.[46] In addition, the MgB/C electrode showed the largest integrated area under the CV curve, implying that it has the maximal specific capacitance, and probably the best electrosorption performance among these electrodes.

Furthermore, the well-defined triangled and nearly symmetric galvanostatic charge-discharge (GCD) curves in Figure S7 revealed that these LMOs/C electrodes possess high reversibility of redox activity during charge/discharge with negligible IR drops in the discharge processes (Figure S7E).[47] The specific capacitances calculated from the discharge profiles after the IR drop exhibited a strong negative correlation with the specific current as expected, and decreased apparently in the order of MgB/C > KB/C > Na/C

8

(Figure S8A). For instance, the specific capacitance of MgB/C is 276.9 F g^{-1} at 0.3 A g^{-1}, greater than those of both NaB/C and KB/C (i.e., 203.0 and 213.5 F g^{-1}, respectively), implying that MgB/C has the maximal salt and/or ion adsorption capacity. The electrochemical impedance spectroscopy (EIS) results (Figure S8B) suggest that MgB/C has the smallest charge-transfer resistance (R$_{ct}$) of 1.4 Ω (*cf*. 2.21 and 1.84 Ω for NaB/C and KB/C, respectively), indicating the highest charge transfer rate at the interface of the MgB/C electrode and the electrolyte. The slope of the straight lines is positively correlated to the interfacial ion migration from the electrolyte to the electrode. Note that the slopes decline in the order of MgB/C > KB/C > NaB/C (see the top left inset in Figure S8B), confirming that MgB/C has the highest interfacial ion migration rate among these electrodes, and thereby the best capacitive performance. [34, 48]

Capacitive Deionization Performance.

The deionization performance of these LMOs/C electrodes was evaluated based on batch-mode MCDI experiments in feed saline with diverse ions (i.e., Na$^+$, K$^+$, Mg^{2+}, Ca^{2+}, and Cu^{2+}). It was noted that the pristine NaB/C electrode exhibited no affinity for Cu^{2+} when 0 V was applied between the two symmetric electrodes in feed saline containing 100 mg L^{-1} (100 ppm, 1573.8 μmol L^{-1}) Cu^{2+} (i.e., the static adsorption process, Figure S9), indicating that the static adsorption of ions was negligible compared to the electrosorption during the MCDI operation. This is mainly due to the presence of the ion-exchange membranes which prevented ions from transporting across the membrane into the electrode regions without a driving force (e.g., a cell potential).[49] When a cell potential of 1.2 V was applied in the MCDI cell with a feed saline of 100 mg L^{-1} Cu^{2+} (i.e., the electrosorption process), the Cu^{2+} went across the membrane rapidly and were attracted by the electrodes, leading to a decline of 38% in Cu^{2+} concentration of the saline stream in ~ 500 seconds (Figure S9). Additionally, the NaB/C electrode can be efficiently regenerated upon reversing the cell potential for 160 seconds, demonstrating fast desorption kinetics.

The LMOs/C electrodes were first tested at 1.2 V in the MCDI cell containing 500 mg L^{-1} (500 ppm) of NaCl as the feed saline. As shown in Figure 2A, the MgB/C electrode exhibited a more rapid decrease in the salt concentration of the saline stream than other LMOs/C electrodes, implying the fastest Na$^+$ adsorption rate of MgB/C among these LMOs/C electrodes (Figure 2B). Besides, MgB/C demonstrated the largest adsorption capacity (59.9 mg g^{-1}) than other birnessite/C electrodes (i.e., HT-NaB/C, NaB/C, and

9

KB/C) under the same circumstances (Figure 2A), which could be attributed to the largest interlayer spacing in MgB (see Figure 1A−1B) allowing for the greatest amount of Na^+ ions to be intercalated.[32] Note that both the Na^+ adsorption capacity and Na^+ adsorption rate of these LMOs/C electrodes were positively correlated to the interlayer spacing of the pristine LMOs (Figures 1B, 2B), in good agreement with previous reports.[31, 32] In addition, all the LMOs/C electrodes demonstrated higher SACs for Na^+, which greatly outstrip most of the manganese oxide/carbon-based electrodes applied for CDI (Table S2). This could be mainly ascribed to the presence of the ion-exchange membranes, which enhanced the charge storage performance of MCDI cells and thereby significantly improved their deionization performance compared to that of CDI.[49]

Extended applications of these LMOs/C electrodes for capacitive removal of alkaline, alkaline-earth, and heavy metal ions (e.g., K^+, Mg^{2+}, Ca^{2+}, and Cu^{2+}) revealed that the deionization performance over these LMOs/C electrodes followed the same trends as observed in the case of 500 ppm NaCl saline, with the orders of both the SACs and the salt and/or ion adsorption rates of MgB/C > KB/C > NaB/C (Figures 2, S10−S13, and Tables S2, S3). To compare the exact deionization performance of the LMOs/C electrodes in the feed saline containing salts with different molar masses, the salt adsorption capacities were normalized by the molar mass of each salt and presented in $\mu mol\ g^{-1}$ (Table S3). All LMOs/C electrodes exhibited a greater SACs (in $\mu mol\ g^{-1}$) in feed saline containing alkaline metal ions (i.e., Na^+ and K^+) than in saline containing alkaline-earth and/or heavy metal ions (i.e., Mg^{2+}, Ca^{2+}, and Cu^{2+}). This is probably attributed to the fact that the singly charged Na^+ and/or K^+ ions with smaller hydrated radii diffused more facilely in the interlayer region of LMOs structure, as compared to the doubly charged ions with larger hydrated radii (i.e., Mg^{2+}, Ca^{2+}, and Cu^{2+}).[32, 50]

Note that the SACs (in $\mu mol\ g^{-1}$) of MgB/C for all metal ions studied, compared to those of NaB/C electrode, have been greatly enhanced after expanding the interlayer spacing of the pristine NaB via ion exchange and thereby being transformed to MgB (Table S3). The enhancement% for Na^+, K^+, Mg^{2+}, and Ca^{2+} were 10.3%, 23.8%, 21.1%, and 20.7%, respectively. Interestingly, the SAC (in $\mu mol\ g^{-1}$) of MgB/C for Cu^{2+} in a 500 ppm of $CuCl_2$ saline has been improved by 52.1% compared to that of NaB/C. This could be likely attributed to the higher affinity of Mg-buserite for Cu^{2+} than that for alkaline and alkaline-earth

10

228   metal ions.[51] Moreover, the SACs of these LMOs/C electrodes for Cu^{2+} ions in a 500 ppm of $CuCl_2$ feed

229   saline outperformed remarkably other CDI electrode materials reported in the literature (Table S4, Figure

230   2D), demonstrating that our electrochemical systems could be a promising platform for copper ions-
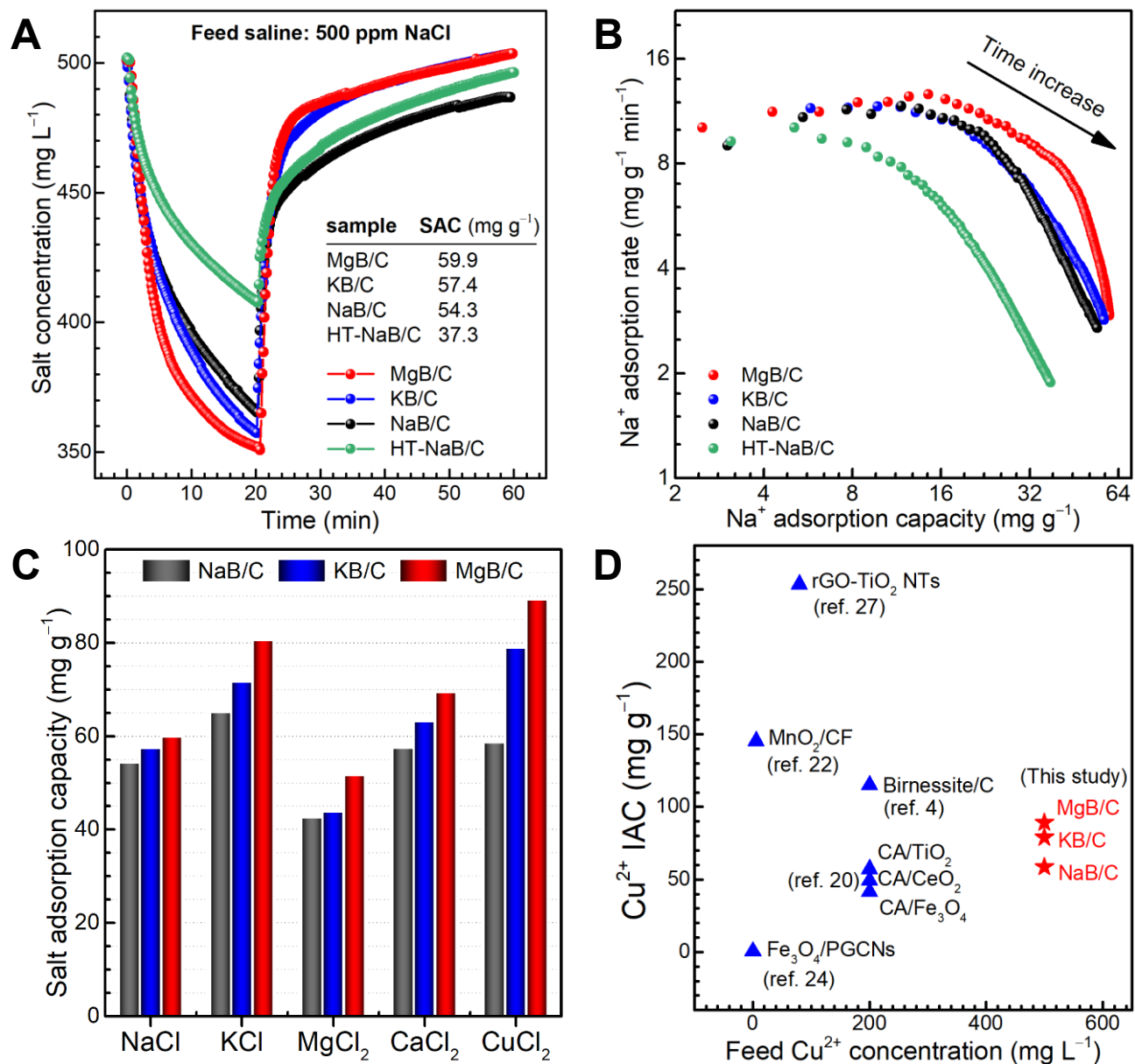
231   containing wastewater remediation.

232

Figure 2. (**A**) Plots of salt concentration versus time in the 3rd run of MCDI operation with the LMOs/C electrodes in a 500 ppm NaCl saline; (**B**) the corresponding Kim-Yoon plots; (**C**) SACs of the LMOs/C electrodes in 500-ppm saline with different salts; and (**D**) comparison of Cu^{2+} IACs of metal oxide-based electrodes applied for CDI.

Effects of Working Voltage, and Feed Concentration on the Capacitive Removal of Copper Ions.

To optimize the deionization performance for Cu^{2+} ions, the LMOs/C electrodes were further tested over a set of cell potentials in feed saline of $CuCl_2$ ranging from 50 to 1000 ppm (371.9−7437.7 μmol L^{-1}). Considering that Cu^{2+} ion is often the target ion of concern due to its greater environmental impact and health risk than Cl^- ion, Cu^{2+} ion adsorption capacity (IAC_{Cu}) rather than SACs, was therefore widely used as one of the key parameters associated with the deionization performance. [4, 6, 12] Note that IACs of these LMOs/C electrodes were positively correlated to the cell potential applied in MCDI operation in the feed saline (Figure S14), in good consistent with other previous reports.[52, 53] Interestingly, the IACs exhibited a confused dependence on the initial salt concentration (C_0) of the $CuCl_2$ saline ranging from 50 to 1000 ppm (Figure S14 A-C), but demonstrated a clear positive correlation with C_0 in the range of 50−200 ppm (Figure S14 D). This is likely due to the side reactions during the MCDI operation at higher cell potentials (e.g., > 1.2 V) in saline with higher $CuCl_2$ concentration (i.e., > 500 ppm).[] Moreover, *in situ* monitoring of the solution pH during the desalination operation over the MgB/C electrode in 1000 ppm of $CuCl_2$ saline (Figures S15) demonstrated a stable desalination behavior (i.e., pH changes were less than 1 unit) of the MgB/C electrode in terms of solution pH when the cell potentials were in the range of 0.8 − 1.2 V. When the cell potential increased up to 1.4 V, the solution pH changed within the range of 3.0 − 5.0, which is likely attributed to the widely reported parasitic side reactions at the surface of the carbon constituent in MgB/C electrode associated with the cathodic reduction of O_2.[52, 54] A small pH change in the solution during the CDI operation must be beneficial for the long-term operation and thus the overall desalination performance of the electrodes.[51] To this end, a cell potential of 1.2 V was adopted as the optimal working voltage (Figure S16) just like it has been widely used by the CDI community (Tables S2, S4). These LMOs/C electrodes demonstrated the best deionization performance at 1.2 V in terms of Cu^{2+} ion adsorption capacities in saline of 500, 500, and 200 ppm $CuCl_2$ for NaB/C, KB/C, and MgB/C, respectively (Figure S16). Therefore, a solution with 100 ppm of Cu^{2+} (equivalent to 211.6 ppm of $CuCl_2$) was selected as the feed saline to further evaluate the desalination behaviors of these LMOs/C electrodes.
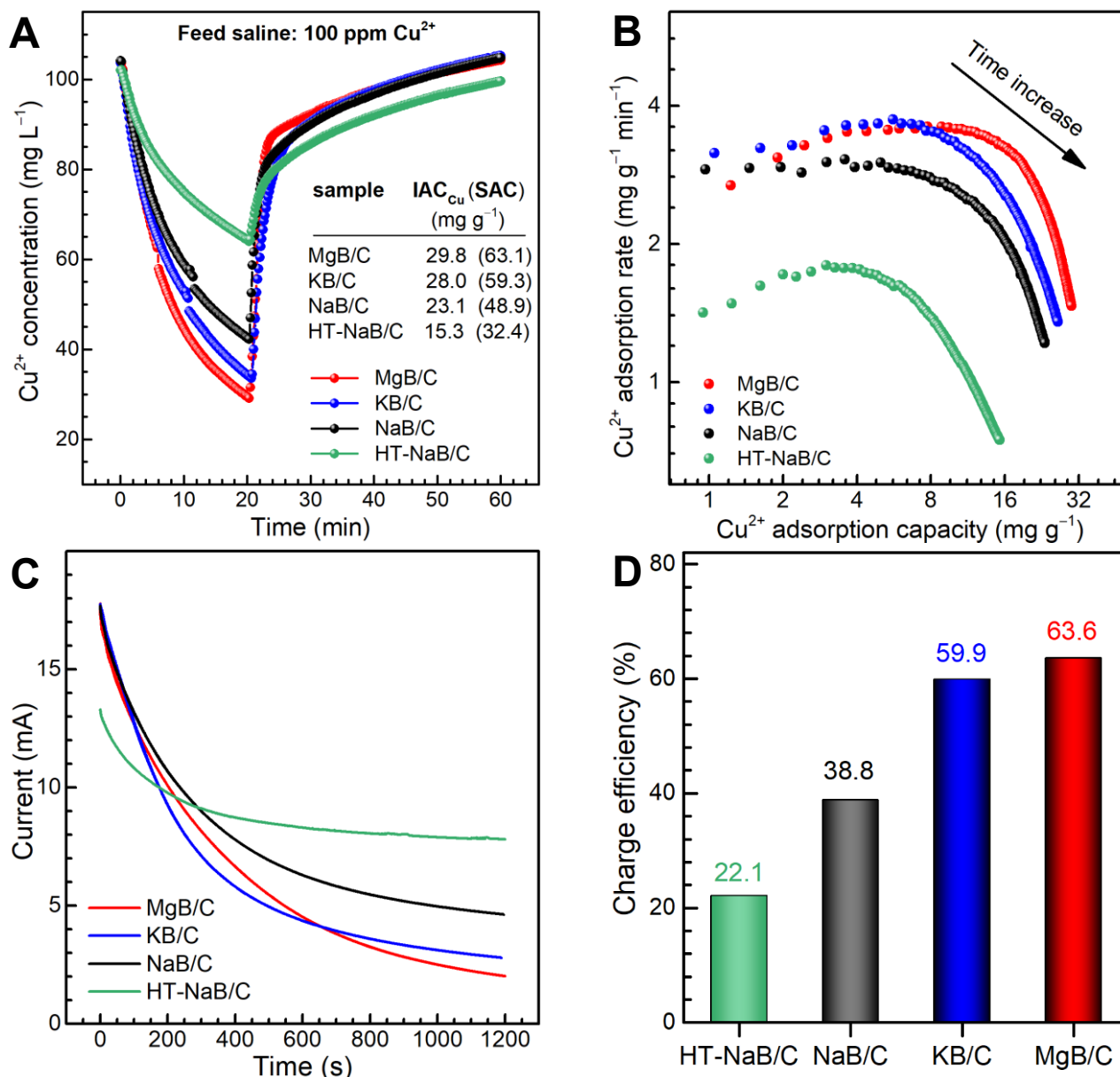
Figure 3. (**A**) Plots of Cu^{2+} concentration versus time in the 3rd run of MCDI with the LMOs/C electrodes in a 100 ppm Cu^{2+} saline; (**B**) the corresponding Kim-Yoon plots; (**C**) plots of the response currents versus time during the desalination operation; and (**D**) the charge efficiency of the LMOs/C during the charging process in a 100 ppm of Cu^{2+} saline.

259

Evaluation of desalination behaviors of these LMOs/C electrodes in feed saline with 100 ppm Cu^{2+} revealed that the MgB/C electrode exhibited the best deionization performance for Cu^{2+} in terms of ion adsorption capacity, rate, and charge efficiency, followed by KB/C, NaB/C, and HT-NaB/C (Figure 3), consistent with the above observations in 500 ppm feed saline with mono- and divalent cations (Figures 2, S10−13). The cycling stability of the electrodes tested in saline of 100 ppm Cu^{2+} at 1.2 V/ −1.2 V
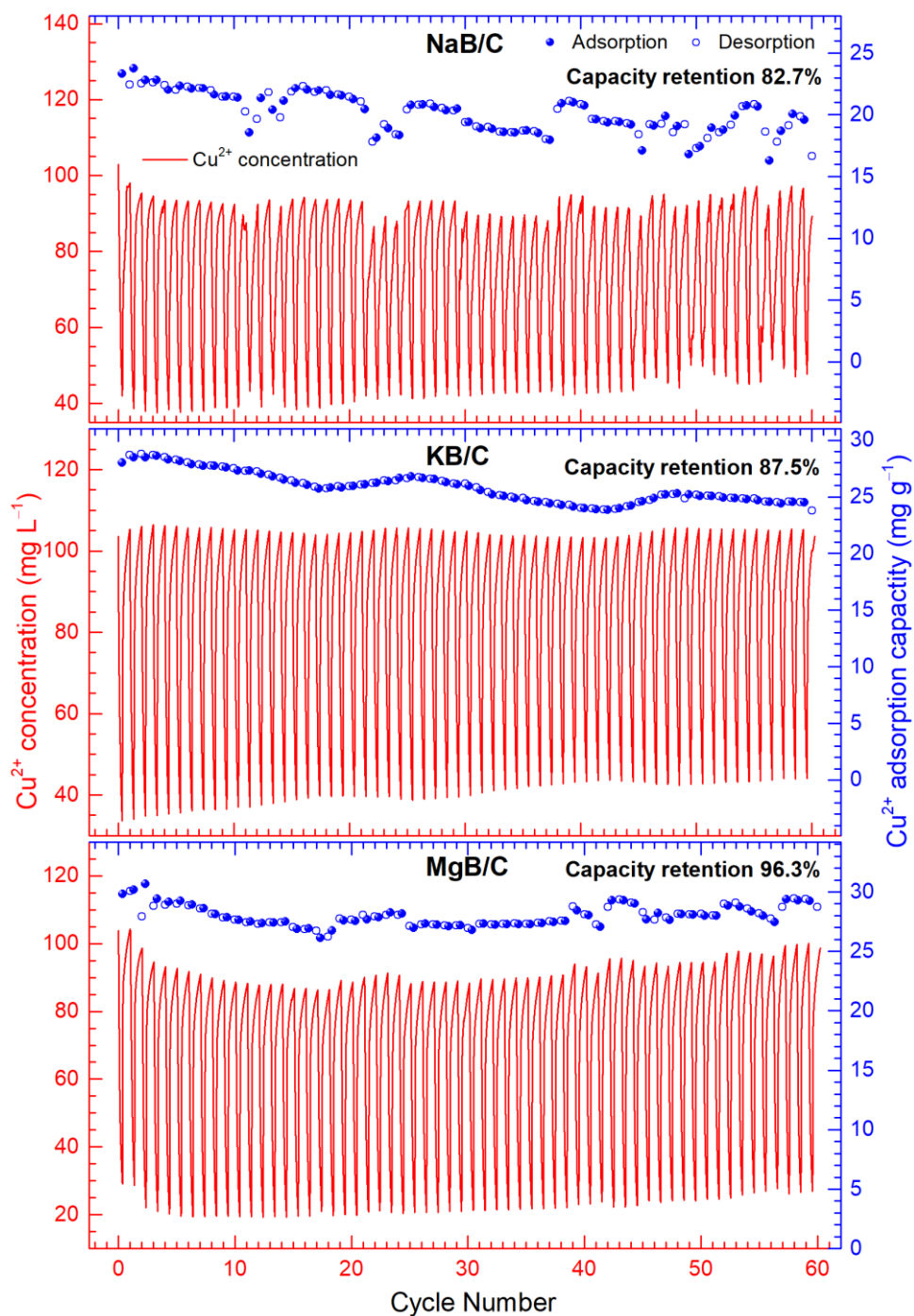
13

Figure 4. Cycling stability and the Cu^{2+} adsorption-desorption capacity of NaB/C, KB/C, and MgB/C electrodes in saline of 100 ppm Cu^{2+} at a cell potential of 1.2 V or −1.2 V.

265

266   unveiled that all electrodes exhibited high reversibility of the adsorption-desorption process for 60

267   consecutive electrosorption and desorption cycles (Figure 4), and that the MgB/C electrode demonstrated

268   superior cycling stability followed by KB/C and NaB/C electrodes in terms of the IAC retention (Figure 4,

14

and Table S5). For instance, the NaB/C electrode showed poor cycling stability with the IAC fluctuating within the range of 16.3−23.7 mg g^{-1} in the cycling test (Figure 4), leading to an IAC recession of 17.3% for 60 consecutive cycles (Table S5). The loss in IAC of the NaB/C electrode was likely attributed to the increasing disorder of lamellar stacking in the MnO_6 octahedra layers derived from the highly frequent intercalation and deintercalation of ions.[31, 34] Besides, the oxidation of the carbon constituent in the cathode (NaB/C) would also contribute in part to the decay of Cu^{2+} ion adsorption capacity.[34, 55] In contrast, after 60 consecutive intercalation-deintercalation of Cu^{2+} cycles, the MgB/C electrode demonstrated an IAC retention as high as 96.3% (Table S5), although a minor fluctuation in IACs was observed along with the Cu^{2+} ion adsorption/release cycles (Figure 4).

Mechanisms for Copper Ions Sequestration.

To understand the mechanism of Cu^{2+} removal on these LMOs/C electrodes, structural changes of the electrodes before and after the cycling tests were investigated ex-situ via XRD characterization. It is worth noting that a new peak at $2\theta = 26.7°$ assignable to the (021) reflection of the PVDF binder appeared in the profiles of all electrodes as expected, and that mixing with PVDF binder and amorphous carbon black for the preparation of the electrode depressed the intensity of all reflections of LMOs (Figures 5A, S17). Similar phenomena were also observed elsewhere. The diffraction pattern of NaB/C electrode after 60 cycles showed evident changes compared to that of the pristine electrode (Figure S17A), i.e., the emergence of some new reflections likely attributed to Cu-buserite,[56] the d_{001} spacing of the pristine NaB decreased slightly from 7.18 to 7.10 Å along with the pronounced decrease in the intensity of all reflections of the pristine NaB. The change in d_{001} spacing of NaB is likely due to the ion exchange of Na^+ with Cu^{2+} from the saline, leading to a transformation of a fraction of Na-birnessite into Cu-birnessite.[57] These observations demonstrate that when NaB/C electrode was cycled in a 100 ppm Cu^{2+} saline, Cu^{2+} ions were intercalated into the interlayer spacing of the pristine NaB during each ion adsorption operation, whereas a fraction of the intercalated Cu^{2+} ions and the original stabilizing Na^+ ions were deintercalated from the interlayer region simultaneously in each ion desorption operation, leading to a gradual structural evolution of Na-birnessite to a mixture of poorly-crystallized Cu-birnessite, Cu-buserite, and the cycled Na-birnessite. [51, 56, 57] The phase transformation is also likely to occur in the cases of KB/C and MgB/C electrodes cycled in Cu^{2+}

15

saline (Figures S17B, 5A), although the peaks corresponding to the Cu-buserite in the XRD pattern of KB/C after 60 cycles are difficult to be identified (Figure S17B). However, considering that Cu-LMOs (i.e., Cu-birnessite, and Cu-buserite) can be easily obtained by ion exchange of Cu^{2+} ions with the Na-LMOs counterparts,[55, 56] and that phase transformations between birnessite and buserite were of common occurrence,[28, 31, 32, 36, 43] it is believed that both Cu-buserite and Cu-birnessite were no doubt formed from the pristine LMOs minerals in the process of cycling the electrodes in Cu^{2+} saline. A decreased d_{001} spacing of 9.40 Å in MgB after cycling in Cu^{2+} saline was observed, which is attributed to the smaller radius of hydrated Cu^{2+} ions compared to that of hydrated Mg^{2+} ions (see Table S3),[32] further confirming the formation of Cu-buserite. Besides, Cu^{2+} ions have also demonstrated a high stabilizing power on LMOs minerals via surface adsorption/complexation, by which the surface energy of the LMOs decreases, thereby improving the thermodynamic stability of LMOs.[51] Therefore, the mechanisms of the LMOs/C electrodes sequestrated Cu^{2+} from solution are likely involved in the intercalation (i.e., redox reactions) with the LMOs minerals and the surface adsorption/complexation (Figure 5B).[31, 32]
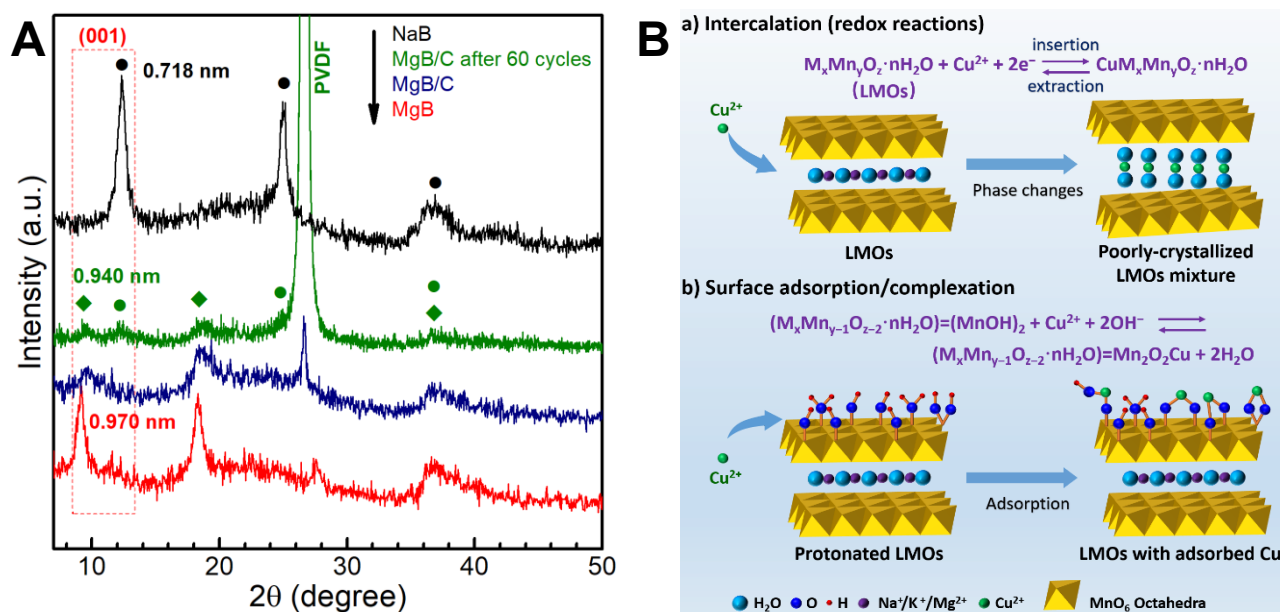

Figure 5. (**A**) XRD patterns of MgB/C electrodes before and after 60 consecutive electrosorption and desorption cycles; (**B**) Schematic illustration of Cu^{2+} removal from saline via both the intercalation (redox reactions) and the surface adsorption mechanisms. Circle (●) represents reflections of Na/Cu-birnessite; diamond (◆) indicates reflections of Mg/Cu-buserite.

310

Environmental Implications.

Layered manganese oxide minerals (e.g., birnessite, and buserite stabilized by alkaline and/or alkaline earth ions) have been demonstrated as one of the most promising redox-active materials for the capacitive deionization platforms towards heavy metal-polluted (e.g., Cu^{2+} ion) water remediation. This study demonstrates a novel strategy for improving the capacitive deionization performance (i.e., enhanced ion adsorption capacity, greater ion adsorption rate, higher charge efficiency, and extended cycling stability) of the MCDI platform toward Cu^{2+} ions by the expansion of the interlayer spacing of the electrode material, i.e., Na-birnessite via ion exchange, which thus transformed Na-birnessite into Mg-buserite. This strategy can be further extended to other redox-active materials applied for CDI towards specific ions. Our results have significant implications for understanding the relationship between the structural parameters of the electrodes and their desalination performance and may pave the way for the rational design of smart electrodes for the large-scale application of CDI towards heavy metal ion sequestration. Given the co-occurring of other metal ions in industrial wastewater, the selectivity of such LMOs electrodes needs to be addressed in future studies.

ASSOCIATED CONTENT

Supporting Information

The Supporting Information is available online and free of charge.

Experimental details; scheme of MCDI setup; XPS spectra, FTIR spectra, SEM images, N_2 adsorption-desorption isotherms, and pore size distribution of the LMOs minerals; CV curves, GCD curves, IR drop plots, specific capacitances plots, and Nyquist plots of EIS of the LMOs/C electrodes; desalination performance curves; Kim-Yoon plots, ion adsorption capacity plots; pH and conductivity plots; contour plots; XRD patterns of LMOs/C electrode before and after cycling in 100 ppm Cu^{2+} saline; comparison of SACs, IACs; cycling stability, and supplementary references.
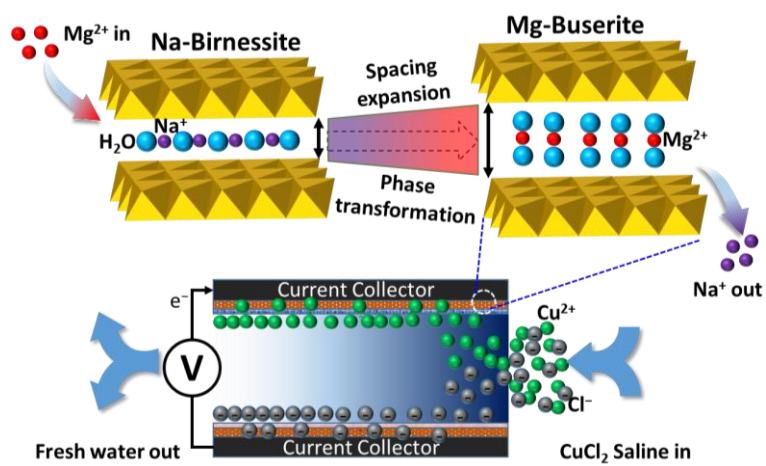
ACKNOWLEDGMENTS

REFERENCES

1. Shannon, M. A.; Bohn, P. W.; Elimelech, M.; Georgiadis, J. G.; Marinas, B. J.; Mayes, A. M., Science and technology for water purification in the coming decades. *Nature* **2008**, *452*, 301-310.

2. Su, X.; Kushima, A.; Halliday, C.; Zhou, J.; Li, J.; Hatton, T. A., Electrochemically-mediated selective capture of heavy metal chromium and arsenic oxyanions from water. *Nat. Commun.* **2018**, *9*, 4701.

3. Huang, C. C.; Su, Y. J., Removal of copper ions from wastewater by adsorption/electrosorption on modified activated carbon cloths. *J. Hazard. Mater.* **2010**, *175*, 477-483.

4. Yang, X.; Liu, L. H.; Tan, W. F.; Qiu, G. H.; Liu, F., High-performance Cu2+ adsorption of birnessite using electrochemically controlled redox reactions. *J. Hazard. Mater.* **2018**, *354*, 107-115.

5. Jin, W.; Hu, M. Q., High-Performance Capacitive Deionization of Copper Ions at Nanoporous ZnS-Decorated Carbon Felt. *J. Electrochem. Soc.* **2019**, *166*, E29-E34.

6. You, S. M.; Tasi, C. K.; Millet, P.; Doong, R. A., Electrochemically capacitive deionization of copper (II) using 3D hierarchically reduced graphene oxide architectures. *Sep. Purif. Technol.* **2020**, *251*, 117368.

7. Al-Saydeh, S. A.; El-Naas, M. H.; Zaidi, S. J., Copper removal from industrial wastewater: A comprehensive review. *J. Ind. Eng. Chem.* **2017**, *56*, 35-44.

8. Oren, Y., Capacitive deionization (CDI) for desalination and water treatment - past, present and future (a review). *Desalination* **2008**, *228*, 10-29.

9. AlMarzooqi, F. A.; Al Ghaferi, A. A.; Saadat, I.; Hilal, N., Application of Capacitive Deionisation in water desalination: A review. *Desalination* **2014**, *342*, 3-15.

10. Suss, M. E.; Porada, S.; Sun, X.; Biesheuvel, P. M.; Yoon, J.; Presser, V., Water desalination via capacitive deionization: what is it and what can we expect from it? *Energy Environ. Sci.* **2015**, *8*, 2296-2319.

11. Maarof, H. I.; Daud, W. M. A. W.; Aroua, M. K., Recent trends in removal and recovery of heavy metals from wastewater by electrochemical technologies. *Rev. Chem. Eng.* **2017**, *33*, 359-386.

12. Chen, R.; Sheehan, T.; Ng, J. L.; Brucks, M.; Su, X., Capacitive deionization and electrosorption for heavy metal removal. *Environ. Sci.- Water Res. Technol.* **2020**, *6*, 258-282.

13. Zhang, X. D.; Zuo, K. C.; Zhang, X. R.; Zhang, C. Y.; Liang, P., Selective ion separation by capacitive deionization (CDI) based technologies: a state-of-the-art review. *Environ. Sci.- Water Res. Technol.* **2020**, *6*, 243-257.

14. Gamaethiralalage, J. G.; Singh, K.; Sahin, S.; Yoon, J.; Elimelech, M.; Suss, M. E.; Liang, P.; Biesheuvel, P. M.; Zornitta, R. L.; de Smet, L. C. P. M., Recent advances in ion selectivity with capacitive deionization. *Energy Environ. Sci.* **2021**, *14*, 1095-1120.

15. Srimuk, P.; Su, X.; Yoon, J.; Aurbach, D.; Presser, V., Charge-transfer materials for electrochemical water desalination, ion separation and the recovery of elements. *Nat. Rev. Mater.* **2020**, *5*, 517-538.

16. Kim, K.; Candeago, R.; Rim, G.; Raymond, D.; Park, A. H. A.; Su, X., Electrochemical approaches for selective recovery of critical elements in hydrometallurgical processes of complex feedstocks. *iScience* **2021**, *24*, 102374.

17. Huang, Z. H.; Yang, Z. Y.; Kang, F. Y.; Inagaki, M., Carbon electrodes for capacitive deionization. *J. Mater. Chem. A* **2017**, *5*, 470-496.

18. Liu, P. Y.; Yan, T. T.; Shi, L. Y.; Park, H. S.; Chen, X. C.; Zhao, Z. G.; Zhang, D. S., Graphene-based materials for capacitive deionization. *J. Mater. Chem. A* **2017**, *5*, 13907-13943.

375   19. Huang, C. C.; He, J. C., Electrosorptive removal of copper ions from wastewater by using ordered mesoporous carbon electrodes. *Chem.*
376   *Eng. J.* **2013**, *221*, 469-475.

377   20. Li, J.; Wang, X. X.; Wang, H. Q.; Wang, S. H.; Hayat, T.; Alsaedi, A.; Wang, X. K., Functionalization of biomass carbonaceous aerogels
378   and their application as electrode materials for electro-enhanced recovery of metal ions. *Environ. Sci.- Nano* **2017**, *4*, 1114-1123.

379   21. Wang, H.; Yan, T. T.; Shen, J. J.; Zhang, J. P.; Shi, L. Y.; Zhang, D. S., Efficient removal of metal ions by capacitive deionization with
380   straw waste derived graphitic porous carbon nanosheets. *Environ. Sci.- Nano* **2020**, *7*, 317-326.

381   22. Hu, C. Z.; Liu, F. Y.; Lan, H. C.; Liu, H. J.; Qu, J. H., Preparation of a manganese dioxide/carbon fiber electrode for electrosorptive
382   removal of copper ions from water. *J. Colloid Interface Sci.* **2015**, *446*, 359-365.

383   23. Liu, Y. H.; Hsi, H. C.; Li, K. C.; Hou, C. H., Electrodeposited Manganese Dioxide/Activated Carbon Composite As a High-Performance
384   Electrode Material for Capacitive Deionization. *ACS Sustain. Chem. Eng.* **2016**, *4*, 4762-4770.

385   24. Zhao, C. J.; Wang, X. L.; Zhang, S. B.; Sun, N.; Zhou, H. J.; Wang, G. Z.; Zhang, Y. X.; Zhang, H. M.; Zhao, H. J., functional porous
386   carbon nanoleaves with Fe3O4 nanoparticles for the capacitive removal of heavy metal ions from water. *Environ. Sci.- Water Res. Technol.*
387   **2020**, *6*, 331-340.

388   25. Mao, M. L.; Yan, T. T.; Chen, G. R.; Zhang, J. P.; Shi, L. Y.; Zhang, D. S., Selective Capacitive Removal of Pb2+ from Wastewater over
389   Redox-Active Electrodes. *Environ. Sci. Technol.* **2021**, *55*, 730-737.

390   26. Wu, S. J.; Yan, P. J.; Yang, W.; Zhou, J.; Wang, H.; Che, L.; Zhu, P. F., ZnCl2 enabled synthesis of activated carbons from ion-exchange
391   resin for efficient removal of Cu2+ ions from water via capacitive deionization. *Chemosphere* **2021**, *264*, 128557.

392   27. Bautista-Patacsil, L.; Lazarte, J. P. L.; Dipasupil, R. C.; Pasco, G. Y.; Eusebio, R. C.; Orbecido, A.; Doong, R., Deionization utilizing
393   reduced graphene oxide-titanium dioxide nanotubes composite for the removal of Pb^{2+} and Cu^{2+}. *J Environ. Chem. Eng.* **2020**, *8*, 103063.

394   28. Wei, W. F.; Cui, X. W.; Chen, W. X.; Ivey, D. G., Manganese oxide-based materials as electrochemical supercapacitor electrodes. *Chem.*
395   *Soc. Rev.* **2011**, *40*, 1697-1721.

396   29. Lee, J.; Kim, S.; Kim, C.; Yoon, J., Hybrid capacitive deionization to enhance the desalination performance of capacitive techniques.
397   *Energy Environ. Sci.* **2014**, *7*, 3683-3689.

398   30. Liu, L. H.; Qiu, G. H.; Suib, S. L.; Liu, F.; Zheng, L. R.; Tan, W. F.; Qin, L. H., Enhancement of Zn^{2+} and Ni^{2+} removal performance using
399   a deionization pseudocapacitor with nanostructured birnessite and its carbon nanotube composite electrodes. *Chem. Eng. J.* **2017**, *328*,
400   464-473.

401   31. Byles, B. W.; Cullen, D. A.; More, K. L.; Pomerantseva, E., Tunnel structured manganese oxide nanowires as redox active electrodes for
402   hybrid capacitive deionization. *Nano Energy* **2018**, *44*, 476-488.

403   32. Byles, B. W.; Hayes-Oberst, B.; Pomerantseva, E., Ion Removal Performance, Structural/Compositional Dynamics, and Electrochemical
404   Stability of Layered Manganese Oxide Electrodes in Hybrid Capacitive Deionization. *ACS Appl. Mater. Interfaces* **2018**, *10*, 32313-32322.

405   33. Leong, Z. Y.; Yang, H. Y., A Study of MnO2 with Different Crystalline Forms for Pseudocapacitive Desalination. *ACS Appl. Mater.*
406   *Interfaces* **2019**, *11*, 13176-13184.

407   34. Jin, J.; Li, M.; Tang, M. T.; Li, Y.; Liu, Y. Y.; Cao, H.; Li, F. H., Phase- and Crystallinity-Tailorable MnO2 as an Electrode for Highly
408   Efficient Hybrid Capacitive Deionization (HCDI). *ACS Sustain. Chem. Eng.* **2020**, *8*, 11424-11434.

409   35. Zhao, Y. B.; Liang, B. L.; Zong, M. Z.; Duan, M.; Li, K. X.; Lv, C. C., Different crystallographic sodium manganese oxides for capacitive
410   deionization: performance comparison and the associated mechanism. *Environ. Sci.- Nano* **2019**, *6*, 3091-3101.

411   36. Post, J. E., Manganese oxide minerals: Crystal structures and economic and environmental significance. *Proc. Nat. Acad. Sci. U.S.A.* **1999**,
412   *96*, 3447-3454.

413   37. Liu, L. H.; Tan, W. F.; Suib, S. L.; Qiu, G. H.; Zheng, L. R.; Huang, Q. Y.; Liu, C. S., Effective Zinc Adsorption Driven by Electrochemical
414   Redox Reactions of Birnessite Nanosheets Generated by Solar Photochemistry. *ACS Sustain. Chem. Eng.* **2018**, *6*, 13907-13914.

415   38. Chen, L.; Shi, G. S.; Shen, J.; Peng, B. Q.; Zhang, B. W.; Wang, Y. Z.; Bian, F. G.; Wang, J. J.; Li, D. Y.; Qian, Z.; Xu, G.; Liu, G. P.;

Zeng, J. R.; Zhang, L. J.; Yang, Y. Z.; Zhou, G. Q.; Wu, M. H.; Jin, W. Q.; Li, J. Y.; Fang, H. P., Ion sieving in graphene oxide membranes via cationic control of interlayer spacing. *Nature* **2017**, *550*, 415-418.

39. Liu, X. M.; Zhang, L.; Gao, X. R.; Guan, C.; Hu, Y. T.; Wang, J., Enlarged Interlayer Spacing in Cobalt-Manganese Layered Double Hydroxide Guiding Transformation to Layered Structure for High Supercapacitance. *ACS Appl. Mater. Interfaces* **2019**, *11*, 23236-23243.

40. Sarkar, D.; Das, D.; Das, S.; Kumar, A.; Patil, S.; Nanda, K. K.; Sarma, D. D.; Shukla, A., Expanding Interlayer Spacing in MoS2 for Realizing an Advanced Supercapacitor. *ACS Energy Lett.* **2019**, *4*, 1602-1609.

41. Wang, S. Y.; Wang, G.; Che, X. P.; Wang, S. F.; Li, C. X.; Li, D. Z.; Zhang, Y. Q.; Dong, Q.; Qiu, J. S., Enhancing the capacitive deionization performance of NaMnO2 by interface engineering and redox-reaction. *Environ. Sci.- Nano* **2019**, *6*, 2379-2388.

42. Feng, Q.; Sun, E. H.; Yanagisawa, K.; Yamasaki, N., Synthesis of birnessite-type sodium manganese oxides by solution reaction and hydrothermal methods. *J. Ceram. Soc. Jpn.* **1997**, *105*, 564-568.

43. Feng, Q.; Kanoh, H.; Ooi, K., Manganese oxide porous crystals. *J. Mater. Chem.* **1999**, *9*, 319-333.

44. Biesinger, M. C.; Payne, B. P.; Grosvenor, A. P.; Lau, L. W. M.; Gerson, A. R.; Smart, R. S., Resolving surface chemical states in XPS analysis of first row transition metals, oxides and hydroxides: Cr, Mn, Fe, Co and Ni. *Appl. Surf. Sci.* **2011**, *257*, 2717-2730.

45. Wachs, I. E., Infrared-Spectroscopy of Supported Metal-Oxide Catalysts. *Colloids Surf., A* **1995**, *105*, 143-149.

46. Lukatskaya, M. R.; Dunn, B.; Gogotsi, Y., Multidimensional materials and device architectures for future hybrid energy storage. *Nat. Commun.* **2016**, *7*, 12647.

47. Brousse, T.; Belanger, D.; Long, J. W., To Be or Not To Be Pseudocapacitive? *J. Electrochem. Soc.* **2015**, *162*, A5185-A5189.

48. Mao, M. L.; Yan, T. T.; Shen, J. J.; Zhang, J. P.; Zhang, D. S., Capacitive Removal of Heavy Metal Ions from Wastewater via an Electro-Adsorption and Electro-Reaction Coupling Process. *Environ. Sci. Technol.* **2021**, *55*, 3333-3340.

49. McNair, R.; Szekely, G.; Dryfe, R. A. W., Ion-Exchange Materials for Membrane Capacitive Deionization. *Acs ES&T Water* **2021**, *1*, 217-239.

50. Yin, J. F.; Takeuchi, E. S.; Takeuchi, K. J.; Marschilok, A. C., Synthetic control of manganese birnessite: Impact of crystallite size on Li, Na, and Mg based electrochemistry. *Inorg. Chim. Acta* **2016**, *453*, 230-237.

51. Yang, P.; Post, J. E.; Wang, Q.; Xu, W. Q.; Geiss, R.; McCurdy, P. R.; Zhu, M. Q., Metal Adsorption Controls Stability of Layered Manganese Oxides. *Environ. Sci. Technol.* **2019**, *53*, 7453-7462.

52. Choi, S.; Chang, B.; Kim, S.; Lee, J.; Yoon, J.; Choi, J. W., Battery Electrode Materials with Omnivalent Cation Storage for Fast and Charge-Efficient Ion Removal of Asymmetric Capacitive Deionization. *Adv. Funct. Mater.* **2018**, *28*, 1802665.

53. Mao, M. L.; Yan, T. T.; Shen, J. J.; Zhang, J. P.; Zhang, D. S., Selective Capacitive Removal of Heavy Metal Ions from Wastewater over Lewis Base Sites of S-Doped Fe–N–C Cathodes via an Electro-Adsorption Process. *Environ. Sci. Technol.* **2021**, *55*, 7665-7673.

54. He, D.; Wong, C. E.; Tang, W. W.; Kovalsky, P.; Waite, T. D., Faradaic Reactions in Water Desalination by Batch-Mode Capacitive Deionization. *Environ. Sci. Technol. Lett.* **2016**, *3*, 222-226.

55. Gao, X.; Omosebi, A.; Landon, J.; Liu, K. L., Surface charge enhanced carbon electrodes for stable and efficient capacitive deionization using inverted adsorption-desorption behavior. *Energy Environ. Sci.* **2015**, *8*, 897-909.

56. Feng, X.; Zhao, H.; Liu, F.; Cui, H.; Tan, W.; Li, W., Transformation from Phyllomanganates to Todorokite under Various Conditions: A Review of Implication for Formation Pathway of Natural Todorokite. In *ACS Symp. Ser.*, American Chemical Society: Washington, DC, **2015**; Vol. 1197, pp 107-134.

57. Li, Y. R.; Marschilok, A. C.; Takeuchi, E. S.; Takeuchi, K. J., Synthesis of Copper Birnessite, CuxMnOy·nH2O with Crystallite Size Control: Impact of Crystallite Size on Electrochemistry. *J. Electrochem. Soc.* **2016**, *163*, A281-A285.

455 **TOC Graph**

456